Heliyon 10 (2024) e37538

Contents lists available at ScienceDirect

Heliyon

journal homepage: www.cell.com/heliyon

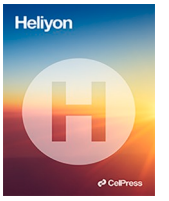

Research article

Insights into bacterial interactions: Comparing fluorine-containing 1,2,4-triazoles to antibiotics using molecular docking and molecular dynamics approaches

Nataliya Korol [a,*], Oksana Holovko-Kamoshenkova [a], Ruslan Mariychuk [b], Mykhailo Slivka [a]

[a] Organic Chemistry Department, Educational and Research Institute of Chemistry and Ecology, Uzhhorod National University, Fedyntsa st. 53/1, Uzhhorod 88000, Ukraine
[b] Department of Ecology, Faculty of Humanities and Natural Sciences, University of Presov, 17 Novembra st. 15, Presov 08001, Slovakia

ARTICLE INFO

Keywords:
1,2,4-Triazol-3-thione
per-fluoralkyl
Molecular docking
Molecular dynamics
Staphylococcus aureus
Serratia marcescens
Bactericide

ABSTRACT

Understanding the interactions between drugs and enzymes is crucial for designing effective therapeutics. This study employed a combination of molecular docking and molecular dynamics (MD) simulations to evaluate the binding affinity, stability, and dynamic behavior of two new compounds (compound **1** and compound **2**) compared to vancomycin and meropenem against *Staphylococcus aureus and Serratia marcescens* bacterial enzymes. Molecular docking studies provided insights into the binding interactions and affinities of these compounds, revealing that both compound **1** and compound **2** exhibit promising binding profiles. In particular, compound **1** demonstrated lower binding energies with key enzymes from *Staphylococcus aureus* compared to vancomycin, suggesting enhanced potential. MD simulations further elucidated the dynamic stability of these complexes. Results indicated that compound **1** maintains consistent binding modes with low RMSD and RMSF values, implying stable interactions. In contrast, vancomycin exhibited high RMSD and RMSF values in some enzyme complexes, reflecting potential instability. Compound **2** showed competitive stability and binding behavior compared to meropenem, with comparable RMSD and RMSF values across various enzyme targets. These findings highlight the potential of compound **1** and compound **2** as viable candidates for further development, offering insights into their stability and efficacy as new therapeutic agents.

1. Introduction

The search for new therapeutic agents to combat bacterial infections remains an urgent priority, given the escalating problem of antibiotic resistance [1–4]. Traditional antibiotics are becoming less effective, necessitating the exploration of alternative therapeutic compounds. In this context, various functionalized synthetic organic substances have emerged as particularly promising candidates [5–7]. These compounds are characterized by their structural diversity, availability, and ease of production, making them potential alternatives to conventional drugs that may no longer produce the desired therapeutic effects.

* Corresponding author.
E-mail addresses: nataliya.korol@uzhnu.edu.ua (N. Korol), miravo2009@gmail.com (O. Holovko-Kamoshenkova), ruslan.mariychuk@unipo.sk (R. Mariychuk), mikhailo.slivka@uzhnu.edu.ua (M. Slivka).

https://doi.org/10.1016/j.heliyon.2024.e37538
Received 17 August 2024; Accepted 4 September 2024
Available online 6 September 2024

Heterocyclic chemistry offers a plethora of valuable compounds, with biological activity serving as a key indicator of their potential efficacy [8–10]. This trend prominently features the triazole ring, known for its robust biological properties, pharmaceutical relevance, and adaptable synthesis routes [11–14]. Among these, mononuclear and fused derivatives of 1,2,4-triazole have gained significant attention as potent agents against a variety of infections and diseases [15–21].

In our previous research, we successfully synthesized both alkylated and fused 1,2,4-triazole derivatives exhibiting notable antibacterial activity [22–24]. Using a cost-effective, efficient, and straightforward electrophilic cyclization methodology [25,26], we obtained a broad spectrum of fused 1,2,4-triazolium salts [27–29]. These compounds demonstrated promising antimicrobial properties, suggesting their potential as therapeutic agents.

The current study aims to perform a comprehensive in silico analysis of bioactive fluorine-containing 1,2,4-triazoles, comparing them with well-known antibiotics such as vancomycin [30,31] and meropenem [32]. Our objective is to evaluate the feasibility of these fluorine-containing triazoles as antibiotic analogs. The focus is on key target organisms, specifically *Staphylococcus aureus* [33] and *Serratia marcescens* [34], which exhibited significant inhibition in microbiological evaluations of the tested fluorine-containing triazoles [35,36].

By integrating experimental quantitative microbiological assays with in silico molecular docking and molecular dynamics simulations, this research aims to elucidate the interaction characteristics of the tested compounds in comparison with established antibiotics. This multifaceted approach is essential for identifying the potential of these compounds as effective therapeutic candidates, a method widely adopted in the development of new, highly effective therapeutic agents [37–41].

The inclusion of computational methods in this study is crucial for deciphering the complex molecular mechanisms underlying the observed antimicrobial activity. This study seeks to uncover the intricacies of the interactions between the compounds and critical bacterial enzymes, thereby shedding light on their mechanisms of action. Specifically, the study will assess the effects of these compounds on enzymes characteristic of *Staphylococcus aureus* and *Serratia marcescens*, providing deeper insights into bacterial pathogenicity, cell wall biosynthesis, and protein production.

This investigation will explore the potential for synergistic effects when combining fluorine-containing triazoles with existing antibiotics. Previous studies have indicated that such combinations can enhance antibacterial efficacy and reduce the likelihood of resistance development. Furthermore, the study will examine the pharmacokinetic and pharmacodynamic properties of these compounds to ensure their suitability for clinical applications.

This approach aims to expand the arsenal of effective therapeutic agents against resistant bacterial strains, addressing a critical need in contemporary medicine. Through detailed in silico and experimental analyses, we aspire to contribute valuable insights into the development of novel antibiotics that can effectively combat the growing threat of antibiotic-resistant bacterial infections.

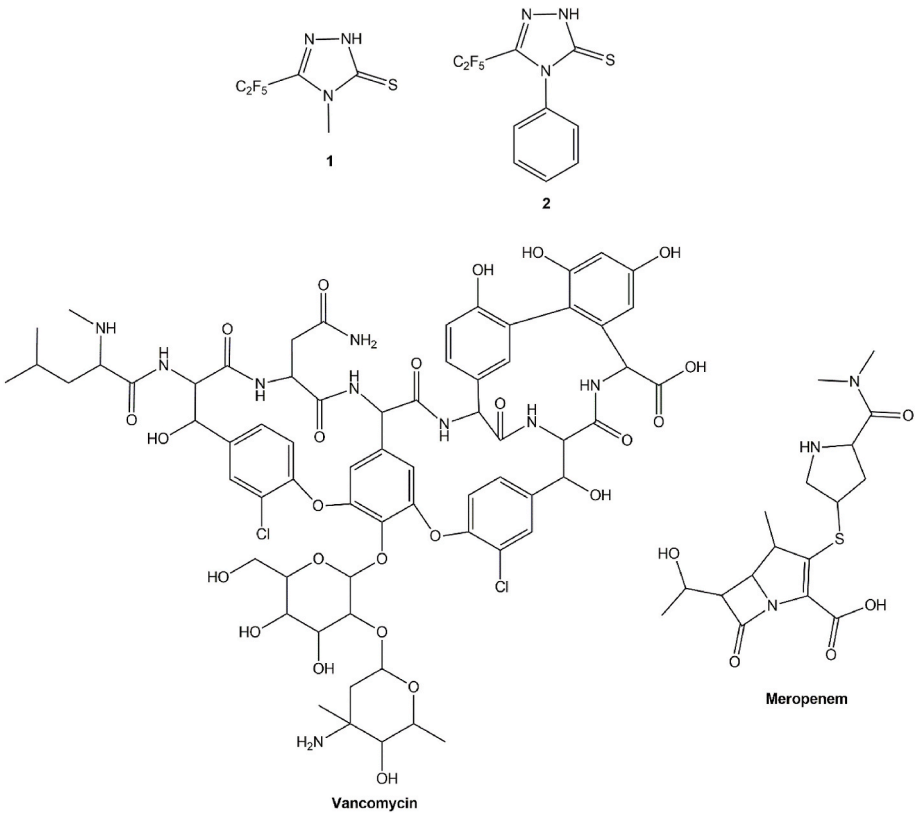

Fig. 1. Molecular formulas of investigated compounds.

2. Computational details

Molecular docking studies of compounds **1** and **2** that were docked into the crystal structures of proteins with PDB_ID: 1BQB, 1HSK, 1JIJ, 3HO8, 1E15, 1I7S, 6ZZ5 and 7AJQ were carried out using Autodock Vina software [42] an open-source molecular docking software. Firstly, we optimized the structures of enzymes in BIOVIA Discovery Studio Visualizer 2021 [43] (https://discover.3ds.com/discovery-studio-visualizer-download). This optimization process included creating the grid box for each protein, adding charges, and refining the structures. The structures of compounds in Hyper Chem 7 [44] http://www.hypercubeusa.com/). We generated 10 conformations in each docking output by using the advanced Genetic algorithm method in Vina Protein/TP. The molecule input preparations and docking output analysis and visualization were carried out using Discovery Studio software. NAMD (Nanoscale Molecular Dynamics) was used for molecular docking simulation. It was performed to evaluate the binding interactions of three leading comlexes with proteins, according to affinity values. The CHARMM36 force field is used in NAMD software [45]. We created the simulation with a duration of 100 ns (nanoseconds) which corresponds to 5000 steps. For energy minimization, we used the conjugate gradient method. The minimization was done in 100 steps by fixing the backbone atoms. For building input files for ligands, particularly parameter files (.prm), we used the CHARMM-GUI web server [46] https://www.charmm-gui.org/. For the RMSD, RMSF,

Table 1
ADMET results for compounds **1** and **2**.

Characteristic	Compound		
	1	2	Reference
Molecular Weight	233.0	295.02	[54]
Volume	163.044	233.058	[54]
Density	1.429	1.266	[54]
nHA	3	3	[54]
nHD	1	1	[54]
nRot	2	3	[54]
nRing	1	2	[54]
MaxRing	5	6	[54]
nHet	9	9	[54]
fChar	0	0	[54]
nRig	6	12	[54]
Flexibility	0.333	0.25	[54]
Stereo Centers	0	0	[54]
TPSA	33.61	33.61	[54]
BBB	0.902336	1.02578	[55]
	0.449	0.856	[54]
Buffer_solubility_mg_L	870506	31625.7	[55]
Caco2	34.8221	25.4956	[55]
	−4.594	−4.48	[54]
CYP_2C19_inhibition	–	–	[55]
	–	+	[54]
CYP_2C9_inhibition	+	+	[55]
	–	–	[54]
CYP_2D6_inhibition	–	–	[55]
	–	–	[54]
CYP_2D6_substrate	–	–	[55]
	–	–	[54]
CYP_3A4_inhibition	+	+	[55]
	–	–	[54]
CYP_3A4_substrate	–	Weakly	[55]
	–	–	[54]
CYP1A2 inhibitor	–	+	[54]
CYP1A2 substrate	+	–	[54]
HIA	95.563954	96.499488	[55]
	0.005	0.004	[54]
MDCK	78.7954	51.1375	[55]
	2.7e-05	3e-05	[54]
Pgp_inhibition	–	+	[55]
Plasma_Protein_Binding	62.357679	96.372571	[55]
Pure_water_solubility_mg_L	2793.45	53.5537	[55]
Skin_Permeability -	1.89105	1.62749	[55]
SKlogD_value	2.071640	3.698490	[55]
	1.672	2.93	[54]
SKlogS_buffer	0.572120	0.970120	[55]
SKlogS_pure -	1.921510	3.74137	[55]
	−2.646	−3.579	[54]
Lipinski Rule	+	+	[54]
Pfizer Rule	+	+	[54]
Golden Triangle	+	+	[54]

and SASA calculations, we used the vmdICE [47] plug-in downloaded from http://www.meduniwien.ac.at/msi/biosim/bk/a1375/ [48].

3. Results and discussion

3.1. Background of the study

The compounds under investigation, namely compounds **1** and **2** (Fig. 1), were synthesized using a catalyst-free technique as outlined in Ref. [49]. Motivated by their demonstrated biological activity [35,36], we embarked on an in silico study to delve deeper into potential mechanistic insights and assess the viability of employing these novel fluorine-containing 1,2,4-triazole derivatives as potent antibiotic analogs.

To achieve this, we focused on two specific bacterial strains—Staphylococcus aureus and Serratia marcescens—which exhibited the most promising inhibition activity in the biological assays against compounds **1** and **2** [35,36], providing a reasonable contextual for further exploration of their interactions.

Staphylococcus aureus [50] is a pathogen responsible for a wide range of infections, from minor skin conditions to life-threatening diseases such as pneumonia, endocarditis, and sepsis. The versatility of its pathogenicity, coupled with its ability to develop resistance to multiple antibiotics, including methicillin, makes it a critical target for new therapeutic strategies. The prevalence of methicillin-resistant *Staphylococcus aureus* (MRSA) has made it an urgent priority in the search for novel antibiotics that can effectively manage infections where traditional treatments fail.

Serratia marcescens [51] - the second target due to its association with hospital-acquired infections, particularly in immunocompromised patients. This opportunistic pathogen is known for its resistance to several antibiotics, including those commonly used in clinical settings. The rising incidence of *Serratia marcescens* infections, coupled with its resistance profile, underscores the necessity of developing new compounds that can offer effective treatment options against this pathogen.

For comparative purposes, we included two well-established antibiotics commonly employed as the first line of treatment: vancomycin [52] against *Staphylococcus aureus* and meropenem [53] against *Serratia marcescens*. Vancomycin is a glycopeptide antibiotic that inhibits cell wall synthesis and is often used as a last-resort treatment for multidrug-resistant *Staphylococcus aureus* infections. Meropenem, a broad-spectrum carbapenem antibiotic, is effective against a wide range of Gram-negative and Gram-positive bacteria, including resistant strains of *Serratia marcescens*.

Our methodology involved an in silico study based on quantitative microbiological activity assays to validate the potential of compounds **1** and **2**. This approach aims to provide a detailed understanding of these compounds' potential as therapeutic agents. Using computational methods, we sought to identify specific interactions between these compounds and critical bacterial enzymes, thereby shedding light on their mechanisms of action.

3.2. ADMET analysis

At the outset of our study, we conducted ADMET (Absorption, Distribution, Metabolism, Excretion, and Toxicity) profiling for

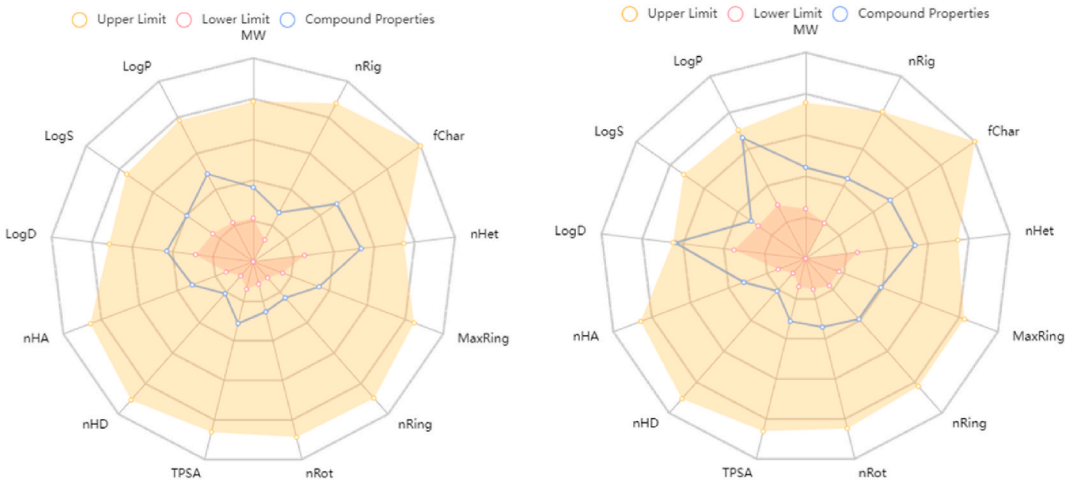

Fig. 2. Physicochemical properties of compound **1** (left) and compound **2** (right) are presented. The properties are as follows: molecular weight (MW), number of rings (nRig), formal charge (fChar), number of heteroatoms (nHet), number of atoms in the biggest ring (MaxRing), number of rigid bonds (nRing), number of rotatable bonds (nRot), topological polar surface area (TPSA), number of hydrogen bond donors (nHD), number of hydrogen bond acceptors (nHA), logarithm of the n-octanol/water distribution coefficients at pH 7.4 (LogD), logarithm of aqueous solubility value (LogS), and logarithm of the n-octanol/water distribution coefficient (LogP). The central blue lines represent the properties of the compounds, fitting within the pink area, which indicates the optimal range for each property.

Compounds **1** and **2** using two distinct tools [54,55]. The summarized results are presented in Table 1 and Physicochemical properties are represented in Fig. 2.

As it is shown from Table 1, compounds **1** and **2** exhibit distinct ADMET profiles, which significantly influence their potential as therapeutic agents. Compound **1** has a molecular weight of 233.0 g/mol and a volume of 163.044 $Å^3$, whereas compound **2** is larger, with a molecular weight of 295.02 g/mol and a volume of 233.058 $Å^3$. The increased molecular weight and volume of compound **2** may affect its pharmacokinetics and its ability to penetrate biological membranes relative to compound **1**.

The densities of the compounds are 1.429 g/cm^3 for compound **1** and 1.266 g/cm^3 for compound **2**. The higher density of compound **1** suggests a more compact molecular structure, which could impact its solubility and stability differently compared to the lower density of compound **2**.

Both compounds possess two hydrogen bond acceptors and one hydrogen bond donor, indicating similar potential for hydrogen bonding interactions. Compound **1** has two rotatable bonds, while compound **2** has three, reflecting greater flexibility which may influence binding dynamics and interactions with targets.

Compound **1** contains one ring with a maximum size of 5 and nine heteroatoms, while compound **2** has two rings with a maximum size of 6 and also nine heteroatoms. The additional ring in compound **2** increases its structural complexity and rigidity, potentially affecting its biological activity and interactions.

Compound **1** has a blood-brain barrier (BBB) penetration score of 0.902336, suggesting moderate potential for central nervous system activity. Compound **2**, with a higher BBB penetration score of 1.02578, may have a greater potential for central nervous system penetration.

Compound **1** demonstrates high buffer solubility (870,506 mg/L) and moderate Caco-2 permeability (34.8221), suggesting excellent formulation potential and oral absorption. In contrast, compound **2**, although highly soluble (31,625.7 mg/L), exhibits slightly lower Caco-2 permeability (25.4956), indicating that its oral absorption might be less efficient compared to compound **1**.

Both compounds inhibit CYP2C9 and CYP3A4, with compound **2** also being a weak substrate for CYP3A4. Compound **1** does not show significant substrate activity for any CYP enzymes, while compound **2**'s inhibition and substrate activity may affect its metabolic stability and drug-drug interactions.

Compound **1** has a plasma protein binding of 62.36 %, while compound **2**'s plasma protein binding is 37.45 %. The lower protein binding in compound **2** suggests a higher proportion of free drug in circulation. Skin permeability is 1.89105 for compound **1** and 1.62749 for compound **2**, indicating a slightly better potential for topical delivery with compound **1**.

Both compounds adhere to the Lipinski and Pfizer rules, indicating favorable drug-like properties. Compound **1** also meets the 'Golden Triangle' criteria, while compound **2** does not.

Compound **1** exhibits a skin sensitization value of 0.005 and an SKlogD value of 2.071640, whereas compound **2** shows a skin sensitization value of 0.004 and an SKlogD value of 3.698490. These values reflect differences in potential skin reactions and lipophilicity. Additionally, compound **2** demonstrates better stability in pure water with a solubility of 53.5537 mg/L compared to 2793.45 mg/L for compound **1**, which may affect its bioavailability and formulation.

In summary, compounds **1** and **2** both display promising ADMET properties. Compound **1** is characterized by greater flexibility and superior skin permeability, while compound **2** has a higher molecular weight, enhanced BBB penetration, and lower plasma protein binding. These differences could impact their efficacy and safety profiles, informing their development and therapeutic applications.

3.3. Molecular docking study

In our study, we conducted molecular docking simulations for compounds **1** and **2**, assessing their interactions with specific enzymes from *Staphylococcus aureus* and *Serratia marcescens*, respectively. These bacteria were selected due to the compounds' notable inhibitory effects observed in preliminary tests [35,36].

For *Staphylococcus aureus*, we focused on four pivotal enzymes that are crucial for the bacterium's virulence and survival. Aureolysin (PDB ID: 1BQB) [56] is a metalloproteinase that plays a fundamental role in the pathogenicity of *Staphylococcus aureus*. It contributes significantly to tissue invasion, immune evasion, and bacterial dissemination by degrading host proteins and interfering with immune responses. The enzyme's unique structure and enzymatic activity make it an appealing target for therapeutic intervention, potentially reducing the bacterium's ability to cause infections.

MurB (PDB ID: 1HSK) [57] is essential for peptidoglycan biosynthesis, which is crucial for maintaining the integrity of bacterial cell walls. Inhibiting MurB disrupts cell wall synthesis, thereby compromising bacterial growth and survival. Given its central role in cell wall assembly, MurB represents a valuable target for antibiotics aimed at tackling *Staphylococcus aureus* infections, which could lead to the development of effective treatments against this common pathogen.

Tyrosyl-tRNA Synthetase (PDB ID: 1JIJ) [58] is responsible for the crucial step of attaching tyrosine to its corresponding tRNA, a process essential for protein synthesis. This enzyme is integral to the translation process, making it critical for bacterial growth. Targeting tyrosyl-tRNA synthetase could impair protein synthesis, providing a strategic approach to inhibit *Staphylococcus aureus* and potentially offering a novel antibacterial strategy.

The Symmetric Tetramer of *Staphylococcus aureus* Pyruvate Carboxylase (PDB ID: 3HO8) [59] plays a key role in gluconeogenesis, a vital metabolic pathway for the bacterium. The enzyme's unique symmetric tetrameric structure underscores its importance in energy metabolism. While further studies are needed to fully elucidate its functional implications, its involvement in metabolic processes highlights its potential as a target for therapeutic intervention, particularly in disrupting bacterial energy production.

These proteins, integral to various aspects of *Staphylococcus aureus* biology, from pathogenicity to metabolic processes re definetely promising targets for novel therapeutic strategies. Their critical roles in bacterial function make them key candidates for drug

development aimed at combating *Staphylococcus aureus* infections.

Similarly, for *Serratia marcescens*, we employed docking and dynamics approaches to investigate interactions with four significant enzymes. Chitinase B (PDB ID: 1E15) [60] is crucial for degrading chitin, a polysaccharide found in fungal cell walls and insect exoskeletons. By breaking down chitin, *Serratia marcescens* can utilize it as a source of carbon and nitrogen, enhancing its survival and pathogenicity. Targeting chitinase B could disrupt this resource utilization, thereby impairing bacterial growth and offering a novel therapeutic avenue.

Anthranilate Synthase (PDB ID: 1I7S) [61] catalyzes the conversion of chorismate and glutamine into anthranilate, a precursor in the biosynthesis of tryptophan, an essential amino acid. The enzyme's role in tryptophan synthesis underscores its importance in bacterial metabolism. Inhibiting anthranilate synthase could disrupt tryptophan production, affecting bacterial growth and providing a potential target for therapeutic intervention.

Serratia marcescens hemolysin (SmhB) (PDB ID: 6ZZ5) [62] is a component of the tripartite alpha pore-forming toxin known as Smh. SmhB plays a crucial role in the toxin's activity, which is responsible for lysing host cells and contributing to the bacterium's virulence. Targeting SmhB could potentially neutralize the toxin's effects, reducing the pathogenic impact of *Serratia marcescens* and offering a strategy to mitigate its virulence.

ExbBD (PDB ID: 7AJQ) [63] is a protein complex involved in regulating active transport systems, including TonB-dependent transporters that import essential nutrients like iron into the bacterial cell. By facilitating nutrient uptake, ExbBD supports bacterial growth and survival. Disrupting ExbBD's function could impair nutrient acquisition, offering a potential method to inhibit *Serratia marcescens* growth.

These enzymes reflect diverse functional mechanisms in *Serratia marcescens*, including resource utilization, toxin production, and nutrient acquisition. Targeting these enzymes with compounds **1** and **2** could offer effective therapeutic strategies against resistant bacterial strains.

Before conducting the molecular docking study, the validation of protein structures was performed using the Ramachandran plot. For this purpose, we utilized the PROCHECK tool [64]. The summarized data from this validation process is presented in Table 2.

The Ramachandran plot statistics for the protein structures show a high percentage of residues in the most favored regions, ranging from 89.0 % to 97.9 %. This indicates that the structures are well-refined and have minimal stereochemical strain. The presence of residues in the additional allowed and generously allowed regions suggests some flexibility in the protein structures, which is typical and acceptable. The very low or absent percentages of residues in the disallowed regions further support the quality of these structures.

The analysis reveals that 1BQB, 1HSK, 1JIJ, and 7AJQ exhibit excellent structural quality, with over 90 % of residues in the most favored regions. 3HO8 and 1E15 also show good structural quality but have slightly lower percentages of residues in the most favored regions, indicating potential areas for minor refinement. 1I7S and 6ZZ5 demonstrate exceptionally high structural accuracy, with the majority of residues in the most favored regions and no residues in disallowed regions (Fig. 3).

Initially, we investigated the interactions between the above-mentioned enzymes of *Staphylococcus aureus* with tested compound **1**, as a promising antibacterial agent, and vancomycin, a widely used antibiotic.

The docking results for compound **1** and vancomycin across various protein targets provide insightful comparisons of their binding affinities and interaction profiles (Table 3). Analyzing these results reveals the nuances of each compound's interaction with different proteins, which can guide further drug development efforts.

For aureolysin, compound **1** exhibits a binding affinity of −5.7 kcal/mol. It interacts through several conventional hydrogen bonds with residues such as HIS148 and ASN167, and also forms halogen (fluorine) bonds with HIS148 and ASN167. Additionally, it engages in Pi-Alkyl interactions with HIS148 and TYR159. Although these interactions are diverse, the overall binding affinity of compound **1** is lower compared to vancomycin. Vancomycin, with an affinity of −8.5 kcal/mol, forms a more extensive network of conventional hydrogen bonds with residues like GLN109, ASN224, and ASP110. It also exhibits a notable Pi-Pi stacking interaction with TYR159 and a Pi-Alkyl interaction with ALA116. The superior binding affinity of vancomycin, coupled with its comprehensive interaction profile, suggests that it binds more effectively to aureolysin than compound **1**. The presence of multiple strong hydrogen bonds and additional non-covalent interactions contribute to vancomycin's higher affinity, demonstrating its potential as a more potent inhibitor of aureolysin.

In the case of MurB, compound **1** shows an affinity of −7.0 kcal/mol and engages in various interactions, including conventional hydrogen bonds with VAL199 and VAL198, halogen bonds, Pi-Sulfur interactions, and Pi-Pi stacking with TYR149. Despite this broad range of interactions, vancomycin exhibits a slightly higher affinity of −8.3 kcal/mol, characterized by numerous conventional hydrogen bonds with residues such as GLU314, THR76, and LYS194, along with an alkyl interaction. The higher binding affinity of vancomycin indicates a more favorable interaction profile with MurB, suggesting that vancomycin may be a more effective inhibitor compared to compound **1**. Vancomycin's ability to form multiple strong hydrogen bonds likely enhances its binding strength and stability at the target site.

For Tyrosyl-tRNA Synthetase, compound **1** demonstrates a binding affinity of −6.5 kcal/mol, with interactions including carbon hydrogen bonds and halogen bonds (Fig. 4). However, vancomycin does not show any binding affinity to this target, indicating that it is not a suitable ligand for tyrosyl-tRNA synthetase (Fig. 5). In contrast, compound **1**'s effective binding suggests its potential as a specific inhibitor for this enzyme, highlighting its unique interaction capabilities in this context.

It might be described by the chemical structure of compound **1**, which is 4-methyl-5-pentafluoroethyl-1,2,4-triazole-3-thione. This possesses structural features such as the triazole ring and the fluorine atoms that may facilitate favorable interactions with the active site of Tyrosyl-tRNA synthetase. The fluorine atoms can engage in specific non-covalent interactions such as halogen bonding [65], which may enhance the binding affinity of compound **1** for the enzyme's active site. Additionally, the triazole ring could provide an optimal fit within the enzyme's binding pocket, leading to a more stable and energetically favorable complex (Fig. 4). The molecular

Table 2
Ramachandran prol statistics.

PDB ID	Most favored regions [A,B,L]		Additional allowed regions [a,b,l,p]		Generously allowed regions [~a,~b,~l, ~p]		Disallowed regions [XX]		Non-glycine and non-proline residues		End-residues (excl. Gly and Pro)	Glycine residues	Proline residues	Total number of residues
	No. of residues	%-tage	No. of residues	%-tage	No. of residues	%-tage	No. of residues	%-tage	No. of residues	%-tage				
1BQB	282	93.7 %	16	5.2 %	3	1.1 %	0	0.0 %	264	100.0 %	2	30	5	301
1HSK	295	92.4 %	17	5.4 %	6	2.2 %	0	0.0 %	279	100.0 %	2	31	7	319
1JIJ	237	90.8 %	21	8.0 %	2	0.8 %	1	0.4 %	261	100.0 %	2	21	11	303
3HO8	3517	89.9 %	328	8.4 %	55	1.4 %	12	0.3 %	3463	100.0 %	19	271	159	3912
1E15	761	89.5 %	85	10.0 %	2	0.2 %	2	0.2 %	850	100.0 %	4	86	52	992
1I7S	1014	92.6 %	81	7.4 %	0	0.0 %	0	0.0 %	1095	100.0 %	9	94	24	1222
6ZZ5	619	97.9 %	13	2.1 %	0	0.0 %	0	0.0 %	632	100.0 %	8	62	14	716
7AJQ	1252	89.0 %	132	9.4 %	22	1.6 %	0	0.0 %	1222	100.0 %	12	96	76	1406

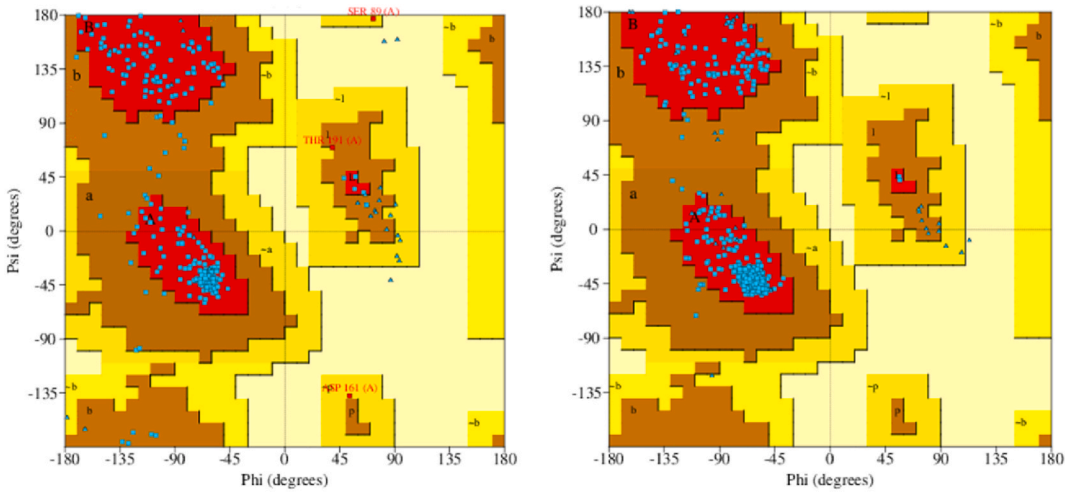

Fig. 3. Ramachandran plots for 1BQB (left) and 6ZZ5 (right).

docking results for various heterocyclic compounds with Tyrosyl-tRNA synthetase consistently indicated that these compounds bind to the same regions of the enzyme, specifically around amino acid residues 35–45 and 160–180 [66–69]. This finding is significant because it demonstrates that these compounds, including compound **1**, interact with key areas of the enzyme's active site, which are crucial for its function.

On the other hand, vancomycin with its large, rigid structure is less suited for interaction with Tyrosyl-tRNA synthetase, which may not provide the appropriate binding pockets or functional groups necessary for vancomycin's effective binding. The absence of significant binding affinity (0.0 kcal/mol) indicates that vancomycin's molecular structure lacks the specific attributes needed to interact strongly with this enzyme.

Regarding Pyruvate Carboxylase, compound **1** has an affinity of −6.1 kcal/mol and interacts through conventional hydrogen bonds, halogen bonds, and various Pi interactions, including Pi-Anion and Pi-Sulfur interactions. Vancomycin, on the other hand, exhibits a significantly higher affinity of −9.4 kcal/mol, with a robust interaction profile that includes extensive conventional hydrogen bonds, Pi-Cation, and Pi-Anion interactions. The stronger binding affinity of vancomycin and its diverse interaction types suggest a more effective binding to Pyruvate Carboxylase compared to compound **1**. Vancomycin's extensive network of interactions contributes to its superior binding strength and potential efficacy as an inhibitor.

Thus, vancomycin demonstrated slightly superior binding affinity values across all tested enzymes compared to compound **1**, with the exception of Tyrosyl-tRNA synthetase, where compound **1** exhibited a binding affinity of −6.5 kcal/mol, whereas vancomycin showed no significant affinity (0.0 kcal/mol). This differential affinity observed between vancomycin and compound **1** for Tyrosyl-tRNA synthetase can be attributed to their distinct molecular structures and modes of interaction with the enzyme.

Vancomycin's ability to form multiple strong conventional hydrogen bonds, as well as additional non-covalent interactions such as π-π stacking and π-cation interactions, enhances its binding profile and effectiveness as an inhibitor (Table 3). Compound **1** also demonstrates promising binding potential through interactions like halogen bonds and π-alkyl interactions. These findings suggest that compound **1** may have potential for specific therapeutic applications, particularly where its unique binding characteristics are advantageous. Further detailed molecular studies and structural analyses are needed to elucidate the specific reasons for these observed differences in affinity and to explore the potential applications of compound **1** in targeted therapeutic contexts.

The docking results for compound **2** and meropenem across various protein targets illustrate distinct differences in binding affinities and interaction profiles (Table 4).

For Chitinase B, compound **2** exhibits a binding affinity of −7.7 kcal/mol. The interactions include carbon hydrogen bonds with TRP220, Pi-Anion interactions with GLU221, and multiple Pi interactions with residues such as PHE190 and PHE191, including Pi-Pi stacked and Pi-Alkyl interactions. The diverse range of interactions, particularly the multiple Pi-Pi stacked and Pi-Alkyl interactions, suggests a robust binding profile for compound **2**. Meropenem demonstrates a binding affinity of −8.0 kcal/mol. It forms conventional hydrogen bonds with residues such as TRP220, GLY480, and GLU221, as well as an additional carbon hydrogen bond.

In the case of Anthranilate Synthase, compound **2** has a binding affinity of −7.0 kcal/mol. It shows a variety of interactions including carbon hydrogen bonds, halogen (fluorine) bonds, and Pi-Anion interactions with residues such as GLY485 and GLN263. The presence of multiple halogen bonds and diverse interaction types indicates a complex binding profile. In contrast, meropenem has a slightly lower affinity of −7.4 kcal/mol but shows fewer interaction types, primarily conventional hydrogen bonds with ARG353 and VAL390 (Fig. 6). While both compounds exhibit strong binding, the extensive range of interactions in compound **2** may suggest a potentially more versatile binding capability, although meropenem's focus on conventional hydrogen bonds still provides a significant binding strength.

For SmhB, compound **2** has a binding affinity of −6.8 kcal/mol and interacts through conventional hydrogen bonds, halogen bonds, Pi-Cation interactions, and Pi-Sigma interactions. The combination of these interactions suggests a varied and potentially effective

Table 3
Molecular docking results for *Staphylococcus aureus* entries with vancomycin and compound **1**.

Protein, PDB ID	Ligand	Affinity, kcal/mol	Residue	Distance, Å	Type
1BQB	**1**	−5.7	HIS148	2,8312	Conventional Hydrogen Bond; Halogen (Fluorine)
			ASN167	2,10041	Conventional Hydrogen Bond; Halogen (Fluorine)
			ASN167	2,65212	Conventional Hydrogen Bond; Halogen (Fluorine)
			ASN156	2,16987	Conventional Hydrogen Bond
			TRP117	3,12632	Carbon Hydrogen Bond
			HIS148	3,14116	Halogen (Fluorine)
			HIS148	3,31793	Halogen (Fluorine)
			ASN167	3,49073	Halogen (Fluorine)
			ASN167	3,1985	Halogen (Fluorine)
			HIS148	4,12987	Pi-Alkyl
			TYR159	4,70217	Pi-Alkyl
1BQB	vancomycin	−8.5	GLN109	2,98709	Conventional Hydrogen Bond
			GLN109	2,99356	Conventional Hydrogen Bond
			ASN224	2,55712	Conventional Hydrogen Bond
			ASN156	2,39187	Conventional Hydrogen Bond
			ASP110	2,91365	Conventional Hydrogen Bond
			TYR159	5,00453	Pi-Pi Stacked
			ALA116	4,08047	Pi-Alkyl
1HSK	**1**	−7.0	VAL199	3526	Conventional Hydrogen Bond; Halogen (Fluorine)
			VAL199	3,50142	Conventional Hydrogen Bond; Halogen (Fluorine)
			VAL199	3,49461	Conventional Hydrogen Bond; Halogen (Fluorine)
			VAL198	3,34188	Carbon Hydrogen Bond; Halogen (Fluorine)
			GLY145	3,24768	Halogen (Fluorine)
			GLY145	3,52965	Halogen (Fluorine)
			LEU197	3,04092	Halogen (Fluorine)
			TYR149	3,85041	Pi-Sulfur
			TYR149	4,19908	Pi-Pi Stacked
			LEU98	5,05157	Alkyl
			VAL198	5,29862	Alkyl
			VAL199	4,84309	Alkyl
1HSK	vancomycin	−8.3	GLU314	2,88673	Conventional Hydrogen Bond
			THR76	1,85269	Conventional Hydrogen Bond
			LYS194	2,38767	Conventional Hydrogen Bond
			ASN189	2,56752	Conventional Hydrogen Bond
			GLU308	2,78735	Conventional Hydrogen Bond
			VAL75	4,6768	Alkyl
			HIS196	4,80326	Pi-Alkyl
1JIJ	**1**	−6.5	ASP40	3,25518	Carbon Hydrogen Bond
			GLN174	3,27867	Halogen (Fluorine)
			GLN174	3,18332	Halogen (Fluorine)
			GLN190	3,14401	Halogen (Fluorine)
			LEU70	4,59259	Alkyl
			TYR36	5,29847	Pi-Alkyl
1JIJ	vancomycin	0.0	–	–	–
3HO8	**1**	−6.1	GLU1063	3,02814	Halogen (Fluorine)
			GLU1067	3,52732	Halogen (Fluorine)
			GLU1063	3,6018	Pi-Anion
			TYR1088	5,75306	Pi-Sulfur
			TYR1088	5,51882	Pi-Pi T-shaped
			ARG1043	2,06519	Conventional Hydrogen Bond
			ARG1043	2,54323	Conventional Hydrogen Bond
			ASP523	2,56938	Conventional Hydrogen Bond
3HO8	vancomycin	−9.4	GLY1045	2,58703	Conventional Hydrogen Bond
			ASN1044	2,42438	Conventional Hydrogen Bond
			TYR524	2,13312	Conventional Hydrogen Bond
			TYR844	3,24958	Carbon Hydrogen Bond
			LYS521	3,52766	Carbon Hydrogen Bond
			ASP523	4,58649	Pi-Cation
			GLU1046	3,9004	Pi-Anion
			GLU885	3,66871	Pi-Anion
			LYS879	3,66136	Pi-Anion
			LYS879	5,03789	Pi-Alkyl

binding profile. Meropenem, with a binding affinity of −7.0 kcal/mol, demonstrates a slightly higher affinity and forms conventional hydrogen bonds with residues such as THR5 and GLN86.

Finally, for ExbBD, compound **2** shows an affinity of −7.5 kcal/mol, characterized by carbon hydrogen bonds, halogen bonds, and several Pi interactions including Pi-Anion and Pi-Alkyl interactions. Meropenem has a higher binding affinity of −8.2 kcal/mol and interacts through carbon hydrogen bonds and several alkyl and Pi-Alkyl interactions.

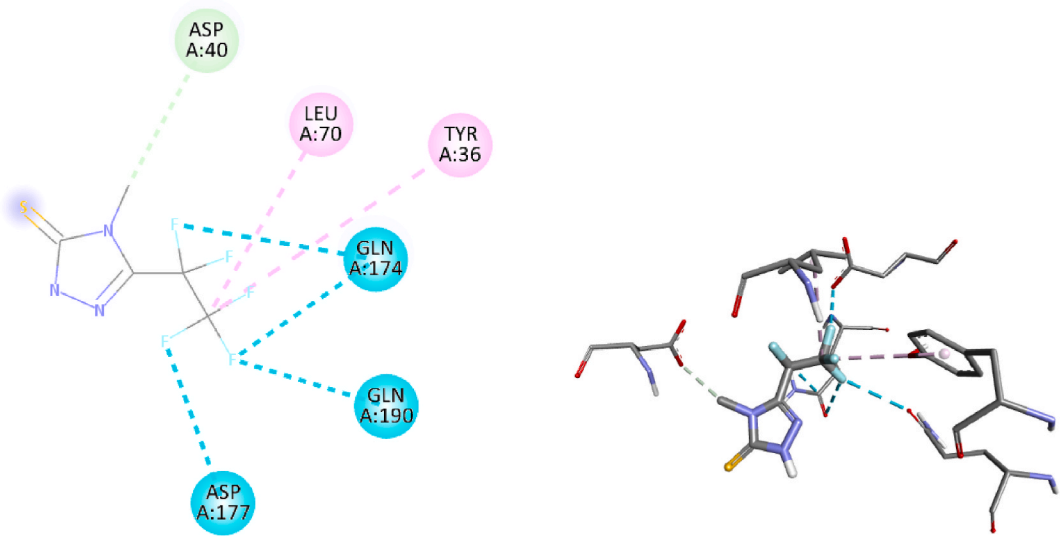

Fig. 4. 2D (left) and 3D (right) visualization of the interaction between Tyrosyl-tRNA synthetase of *Staphylococcus aureus* (PDB ID: 1JIJ) and compound **1**.

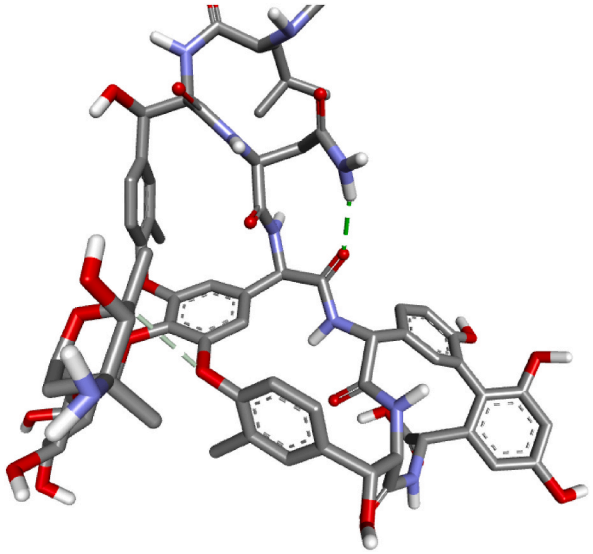

Fig. 5. 3D visualization of the interaction between Tyrosyl-tRNA synthetase of *Staphylococcus aureus* (PDB ID: 1JIJ) and vancomycin.

Of particular interest is the distinct affinity of compound **2** to engage in a greater number of non-covalent interactions, predominantly featuring fluorine atoms (Table 4). This observation highlights the compound's intricate molecular behavior within the enzyme's active site. These findings support the proposition of a novel analogue with promising potential to effectively inhibit *Serratia marcescens*. The nuanced molecular interactions and structural characteristics of this proposed analogue warrant further investigation, with the potential to yield synergistic therapeutic outcomes.

Across different protein targets, meropenem generally exhibits slightly higher binding affinities compared to compound **2**. However, compound **2** demonstrates a diverse range of interactions, including carbon-hydrogen bonds, halogen bonds, and various Pi interactions. This diverse interaction profile suggests that compound **2** has significant potential and deserves further investigation as a new pharmaceutical analogue of meropenem.

3.4. Molecular dynamics simulation

Understanding the dynamic interactions and stability of drug-enzyme complexes is crucial for the development of effective therapeutics. Molecular dynamics (MD) simulations offer a powerful tool to gain detailed insights into these interactions, revealing how

Table 4
Molecular docking results for *Serratia marcescens* entries with meropenem and compound **2**.

Protein, PDB ID	Ligand	Affinity, kcal/mol	Residue	Distance, Å	Type
1E15	**2**	−7.7	TRP220	3,30452	Carbon Hydrogen Bond
			GLU221	4,65104	Pi-Anion
			PHE190	5,20216	Pi-Sulfur
			PHE190	3,96849	Pi-Pi Stacked
			TRP220	4354	Pi-Pi Stacked
			PHE191	5,10713	Pi-Alkyl
			TYR481	5,10277	Pi-Alkyl
1E15	meropenem	−8.0	TRP220	2,62701	Conventional Hydrogen Bond
			GLY480	1,95701	Conventional Hydrogen Bond
			GLU221	2,41751	Conventional Hydrogen Bond
			ASP215	2,50951	Conventional Hydrogen Bond
			TRP220	3,69726	Carbon Hydrogen Bond
1I7S	**2**	−7.0	THR425	2,66072	Carbon Hydrogen Bond; Halogen (Fluorine)
			GLY428	2,58311	Carbon Hydrogen Bond; Halogen (Fluorine)
			GLY485	2,49447	Carbon Hydrogen Bond
			GLY485	2,36781	Carbon Hydrogen Bond; Halogen (Fluorine)
			GLN263	2,96396	Halogen (Fluorine)
			GLN263	3,55859	Halogen (Fluorine)
			GLN263	2,56173	Halogen (Fluorine)
			GLU361	3,2631	Halogen (Fluorine)
			GLY424	3,43858	Halogen (Fluorine)
			GLY424	2,92735	Halogen (Fluorine)
			THR425	2,86189	Halogen (Fluorine)
			GLY485	3,32184	Halogen (Fluorine)
			GLU361	3,88352	Pi-Anion
			VAL265	5,18848	Alkyl
			LEU365	4,79706	Alkyl
			VAL265	5,25322	Pi-Alkyl
			LEU365	5,42868	Pi-Alkyl
1I7S	meropenem	−7.4	ARG353	2,56353	Conventional Hydrogen Bond
			VAL390	2,43523	Conventional Hydrogen Bond
			VAL390	4,62188	Alkyl
6ZZ5	**2**	−6.8	SER273	3,04674	Conventional Hydrogen Bond; Halogen (Fluorine)
			ALA14	3,17108	Halogen (Fluorine)
			SER273	3,89105	Pi-Cation
			SER273	2,99463	Pi-Cation
			ALA178	3,44016	Pi-Sigma
			ALA277	3,85271	Alkyl
			ALA178	5,22058	Pi-Alkyl
6ZZ5	meropenem	−7.0	THR5	2,35771	Conventional Hydrogen Bond
			THR5	2,24928	Conventional Hydrogen Bond
			GLN86	2,4125	Conventional Hydrogen Bond
			SER320	2,56019	Conventional Hydrogen Bond
			SER317	2,75975	Conventional Hydrogen Bond
			GLU291	2,40817	Conventional Hydrogen Bond
7AJQ	**2**	−7.5	GLY258	3,21584	Carbon Hydrogen Bond; Halogen (Fluorine)
			GLY258	3,55758	Carbon Hydrogen Bond; Halogen (Fluorine)
			GLY143	3,31756	Halogen (Fluorine)
			LEU254	3,22324	Halogen (Fluorine)
			LEU254	3,5245	Halogen (Fluorine)
			GLU146	4,61472	Pi-Anion
			LEU254	3,67924	Pi-Sigma
			ARG147	4,30799	Alkyl
			LYS145	5,04235	Alkyl
			LEU254	5,31537	Alkyl
			LYS145	3,96886	Pi-Alkyl
			LYS145	5,40715	Pi-Alkyl
7AJQ	meropenem	−8.2	LEU255	3,61108	Carbon Hydrogen Bond
			GLY149	3,67031	Carbon Hydrogen Bond
			ARG147	4,88289	Alkyl
			ARG151	4,7834	Alkyl
			LEU255	3,89451	Alkyl
			PHE150	4,87493	Pi-Alkyl

molecules behave and interact over time under physiological conditions. By simulating the molecular environment, MD simulations allow us to observe the stability, conformational changes, and flexibility of drug-enzyme complexes, which are essential for predicting the efficacy and potential of therapeutic compounds [70].

In our study, we conducted comprehensive MD simulations to evaluate the stability and flexibility of four different drug-enzyme

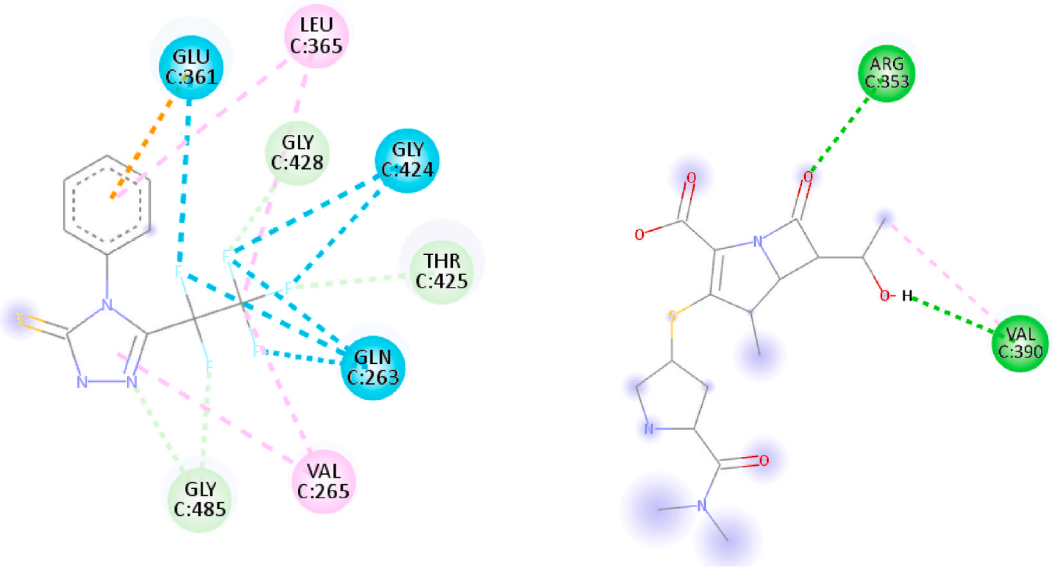

Fig. 6. 2D representation of interactions between 1I7S with compond **2** (left) and meropenem (right).

complexes: compound **1**, compound **2**, vancomycin, and meropenem. These simulations were performed with a specific focus on key enzymes.

The results of MD simulations of compound **1** and vancomycin with enzyme complexes characterized for *Staphylococcus aureus* bacteria are summarized in Table 6.

Unexpectedly, our MD simulations yielded fascinating results. While the RMSD and RMSF values of compound **1** complexes with all four enzymes adhered to expected ranges, the corresponding outcomes for vancomycin complexes with *Staphylococcus aureus* MurB and the Symmetrical Tetramer of *Staphylococcus aureus* Pyruvate Carboxylase demonstrated either remarkable stability (0,2015 and 0,0197) or substantial fluctuation (301,4932 and 14,6529). This suggests that vancomycin might face challenges in forming robust complexes with these enzymes.

In our case, an RMSD of 0,2015 for vancomycin with *Staphylococcus aureus* MurB means that, on average, the positions of corresponding atoms in the simulated vancomycin-MurB complex are about 0,2015 Å away from their positions in the initial crystallographic structure. A low RMSD like this indicates that the complex is relatively stable and that the vancomycin molecule is maintaining a consistent binding mode with the MurB enzyme.

RMSF measures the average fluctuation in the positions of individual atoms within a molecule during a MD simulation. It provides insight into the flexibility and dynamic behavior of the molecule. A lower RMSF value indicates less fluctuation, while a higher value suggests greater movement or flexibility of the atoms.

An RMSF of 0,0197 for vancomycin with MurB means that, on average, the individual atoms in the vancomycin molecule are fluctuating by about 0,0197 Å during the simulation. This low RMSF value suggests that the vancomycin molecule is experiencing relatively minor fluctuations, implying a stable binding mode and limited conformational changes during the simulation.

The combination of a low RMSD and low RMSF for the vancomycin-MurB complex indicates that vancomycin is maintaining a stable binding mode with the MurB enzyme, and the complex is not undergoing significant structural changes or fluctuations during the MD simulation. This stability could be indicative of a strong or well-fitted interaction between vancomycin and MurB in this specific context.

Regarding Aureolysin, there is not a crucial difference in RMSF values observed between compound **1** and vancomycin. As seen in Fig. 4, both complexes became stable at the fifth second of simulation with average values of RMSF 0,32 for compound 1 and 0,30 for

Table 6
Results of MD simulations between *Staphylococcus aureus* entries with vancomycin and compound **1**.

Bacteria	*Staphylococcus aureus*			
PDB ID	1BQB	1HSK	1JIJ	3HO8
Compound	**1**			
RMSD, Å	2,2219	1,8389	2,3711	1,6942
RMSF, Å	0,3213	0,2444	0,3073	0,2862
Antibiotic	**Vancomycin**			
RMSD, Å	1,8505	0,2015	2,2388	301,4932
RMSF, Å	0,2960	0,0197	0,3085	14,6529

vancomycin (Fig. 7).

RMSF of 14,6529 for vancomycin with the Symmetrical Tetramer suggests that, on average, the individual atoms in the vancomycin molecule are fluctuating by approximately 14,6529 Å during the simulation. This relatively high RMSF value indicates that the vancomycin molecule is undergoing significant fluctuations and movements within the complex.

The combination of a high RMSD (301,4932) and a high RMSF (14,6529) for the vancomycin-Symmetrical Tetramer complex suggests that the complex has undergone substantial structural changes and fluctuations during the MD simulation. This could indicate that vancomycin's binding to the Symmetrical Tetramer is not as stable or well-constrained as in other complexes, and the complex might be undergoing dynamic rearrangements or interactions that lead to its fluctuation and divergence from the initial structure.

The Symmetrical Tetramer of *Staphylococcus aureus* Pyruvate Carboxylase complex with vancomycin became stable at the third second of MD simulation, but at seconds 1 and 2, the RMSF values were 158 and 149 Å respectively, resulting in an average RMSF of 14,6529 Å. Comparing with compound **1**, whose complex became stable at the sixth second with no particularities observed, vancomycin's interactions are quite questionable (Fig. 8).

The RMSD of 301,4932 for vancomycin with the Symmetrical Tetramer of *Staphylococcus aureus* Pyruvate Carboxylase means that, on average, the positions of corresponding atoms in the simulated complex are about 301,4932 Å away from their positions in the initial structure. Such a high RMSD value indicates substantial structural divergence between the initial and simulated structures. In other words, the vancomycin-Symmetrical Tetramer complex has experienced significant conformational changes or rearrangements during the MD simulation [71–75].

The MD simulations for compound **2** and the antibiotic meropenem with enzyme complexes from *Serratia marcescens* bacteria yielded the results displayed in Table 7.

Analyzing these results, for all four enzyme complexes, compound **2** demonstrated RMSD values ranging from 1.3877 Å to 2.0024 Å, suggesting that compound **2** maintains relatively stable binding across different enzyme targets, though with some variation. Meropenem showed slightly higher RMSD values compared to compound **2** for the enzyme complexes with Chitinase B, Anthranilate Synthase, and SmhB, indicating a comparable or slightly less stable binding conformation. However, for ExbBD, the RMSD values for both compound **2** and meropenem were close, with compound **2** being slightly higher. Compound **2** displayed RMSF values between 0.2736 Å and 0.3026 Å, indicating moderate fluctuations in atomic positions during the simulations and suggesting that compound **2** remains relatively stable and exhibits consistent binding behavior across different enzyme complexes. Meropenem showed RMSF values in the range of 0.2773 Å to 0.3017 Å, which are very similar to those of compound **2**, implying that both compounds have comparable levels of atomic fluctuation and structural stability during the simulations. The MD simulations indicate that compound **2** has a comparable or slightly more stable binding affinity to the tested enzyme complexes of *Serratia marcescens* compared to the antibiotic meropenem. The RMSD and RMSF values suggest that compound **2** maintains stable binding conformations and exhibits consistent atomic fluctuations across different targets, making it a potential candidate for further investigation as a new pharmaceutical agent.

Our MD simulations have provided valuable insights into the stability and interaction dynamics of drug-enzyme complexes involving compound **1**, compound **2**, vancomycin, and meropenem. For compound **1**, the simulations revealed consistent stability and flexibility across various enzyme targets, with RMSD and RMSF values indicating favorable binding characteristics. In contrast,

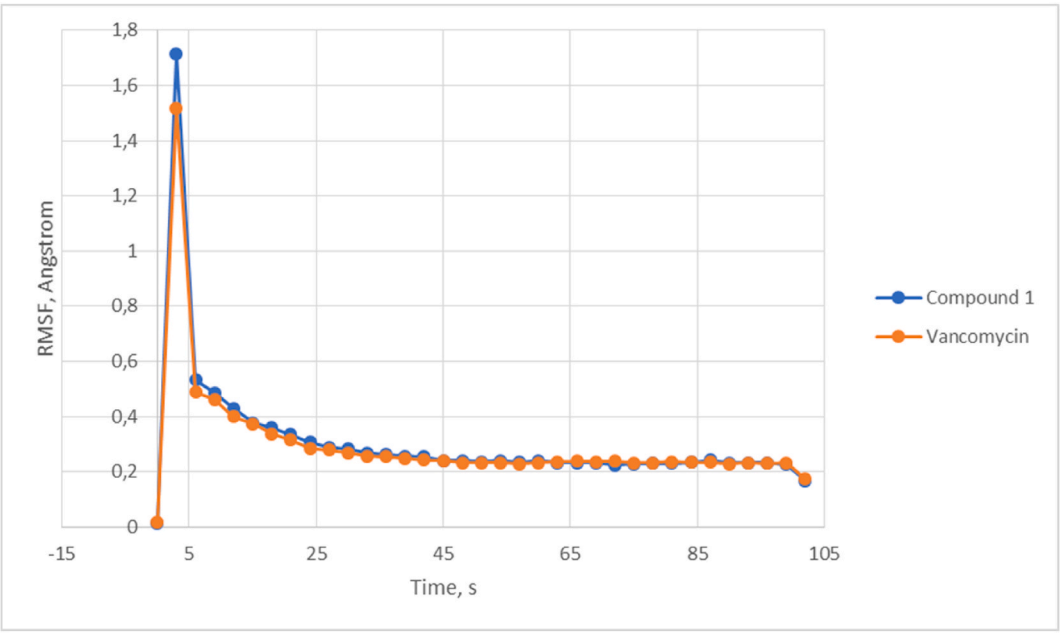

Fig. 7. RMSF curve for complexes of Aureolysin with compound **1** and vancomycin.

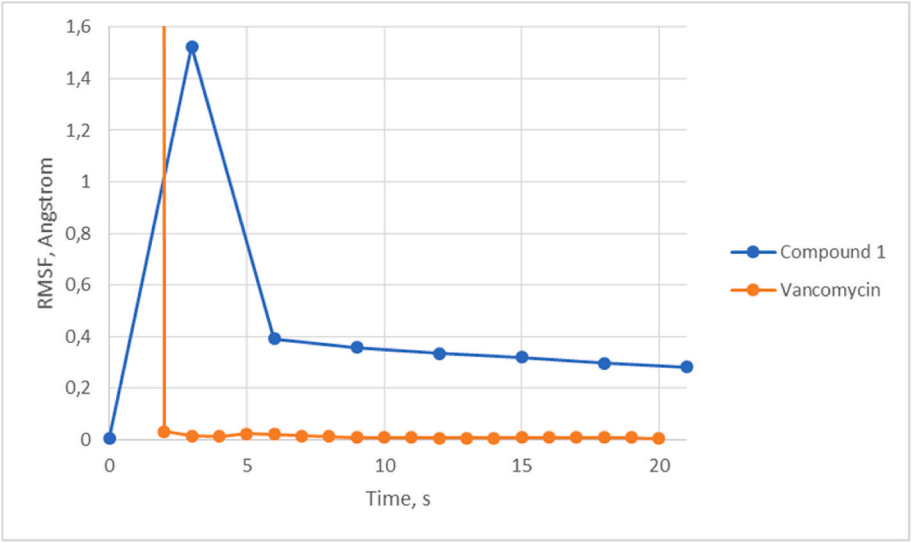

Fig. 8. RMSF curve for complexes of Symmetrical Tetramer of *Staphylococcus aureus* Pyruvate Carboxylase with compound **1** and vancomycin.

Table 7
Results of MD simulations between *Serratia marcescens* entries with meropenem and compound **2.**

Bacteria	*Serratia marcescens*			
PDB ID	1E15	1I7S	6ZZ5	7AJQ
Compound	**2**			
RMSD, Å	1,3877	1,8829	1,7332	2,0024
RMSF, Å	0,2736	0,3026	0,3020	0,2970
Antibiotic	**Meropenem**			
RMSD, Å	1,4164	1,8991	1,6034	1,9810
RMSF, Å	0,2773	0,3017	0,2986	0,3008

vancomycin showed significant variation in stability, particularly with certain enzymes, suggesting potential challenges in forming robust complexes. The observed high RMSD and RMSF values for vancomycin with specific targets point to substantial conformational changes, raising questions about its binding efficacy in these contexts.

Similarly, compound **2** exhibited stable binding conformations with the *Serratia marcescens* enzyme complexes, with RMSD and RMSF values comparable to or slightly better than those of meropenem. These findings suggest that compound **2** maintains consistent binding behavior and stability, positioning it as a promising candidate for further development as a therapeutic agent. Overall, the results underscore the importance of MD simulations in evaluating drug-enzyme interactions and highlight the potential of compound **1** and compound **2** in therapeutic applications.

4. Conclusion

The integration of molecular docking and molecular dynamics simulation approaches has significantly advanced our understanding of the interactions and stability of compound **1** and compound **2** with key bacterial enzymes. Molecular docking analyses indicated that both compounds exhibit substantial binding affinities towards their target enzymes, outperforming vancomycin and meropenem in several instances. This suggests that compound **1** and compound **2** may possess superior binding capabilities, which could translate into enhanced therapeutic effectiveness.

MD simulations further validated these findings by assessing the dynamic behavior and stability of the drug-enzyme complexes over time. Compound **1** demonstrated remarkable stability and consistent binding across a range of bacterial enzyme targets, highlighting its potential as a robust therapeutic agent. In contrast, vancomycin exhibited notable fluctuations in binding stability with certain enzyme complexes, suggesting potential challenges in maintaining a stable interaction in some contexts.

Similarly, compound **2** showed stability levels comparable to meropenem, an established antibiotic. The RMSD and RMSF values indicated that compound **2** maintains a stable binding conformation and exhibits consistent atomic fluctuations across different enzyme targets. This performance suggests that compound **2** could serve as a competitive alternative to meropenem, potentially offering similar or enhanced efficacy against bacterial pathogens.

Overall, the comprehensive data from both molecular docking and MD simulations underscore the promising therapeutic potential of compound **1** and compound **2.** Their superior binding affinities and stability profiles position them as strong candidates for further

development as novel therapeutic agents. Future research should focus on experimental validation of these computational predictions through in vitro and in vivo assays to confirm their effectiveness and safety. Additionally, exploring their potential in clinical settings will be crucial to fully assess their viability as new treatments for bacterial infections.

Funding sources

This research did not receive any specific grant from funding agencies in the public, commercial, or not-for-profit sectors.

Data availability

Data will be made available on request.

CRediT authorship contribution statement

Nataliya Korol: Conceptualization, Data curation, Investigation, Methodology, Software, Supervision, Visualization, Writing – original draft. **Oksana Holovko-Kamoshenkova:** Investigation, Methodology, Resources, Writing – review & editing. **Ruslan Mariychuk:** Validation, Writing – review & editing. **Mykhailo Slivka:** Investigation, Methodology, Validation, Writing – review & editing.

Declaration of competing interest

The authors declare that they have no known competing financial interests or personal relationships that could have appeared to influence the work reported in this paper.

Acknowledgments

This study was partially supported by the National Scholarship Programme of the Slovak Republic (ID 45748, ID 46970).

References

[1] M. Frieri, K. Kumar, A. Boutin, Antibiotic resistance, J. Infect. Public Health 10 (2017) 369–378, https://doi.org/10.1016/j.jiph.2016.08.007.
[2] G. Mancuso, A. Midiri, E. Gerace, C. Biondo, Bacterial antibiotic resistance: the most critical pathogens, Pathogens 10 (2021) 1310–1324, https://doi.org/10.3390/pathogens10101310.
[3] D.C. Nwobodo, M.C. Ugwu, O.C. Anie, M.T.S. Al-Ouqaili, J.C. Ikem, U.V. Chigozie, M. Saki, Antibiotic resistance: the challenges and some emerging strategies for tackling a global menace, J. Clin. Lab. Anal. 36 (2022) 24655, https://doi.org/10.1002/jcla.24655.
[4] R. Urban-Chmiel, A. Marek, D. Stępień-Pyśniak, K. Wieczorek, M. Dec, A. Nowaczek, J. Osek, Antibiotic resistance in bacteria — a review, Antibiotics 11 (2022) 1079–1119, https://doi.org/10.3390/antibiotics11081079.
[5] A. Rusu, I.-M. Moga, L. Uncu, G. Hancu, The role of five-membered heterocycles in the molecular structure of antibacterial drugs used in therapy, Pharmaceutic 15 (2023) 2554–2605, https://doi.org/10.3390/pharmaceutics15112554.
[6] M. Aatif, M.A. Raza, K. Javed, S.M. Nashre-ul-Islam, M. Farhan, M.W. Alam, Potential nitrogen-based heterocyclic compounds for treating infectious diseases: a literature review, Antibiotics 11 (2022) 1750–1775, https://doi.org/10.3390/antibiotics11121750.
[7] E. Kabir, M. Uzzaman, A review on biological and medicinal impact of heterocyclic compounds, Res. in Chem. 4 (2022) 100606, https://doi.org/10.1016/j.rechem.2022.100606.
[8] A.P. Taylor, R.P. Robinson, Y.M. Fobian, D.C. Blakemore, L.H. Jones, O. Fadeyi, Modern advances in heterocyclic chemistry in drug discovery, Org. Biomol. Chem. 14 (2016) 6611–6637, https://doi.org/10.1039/C6OB00936K.
[9] A. Gomtsyan, Heterocycles in drugs and drug discovery, Chem. Heterocycl. Comp. 48 (2012) 7–10, https://doi.org/10.1007/s10593-012-0960-z.
[10] J. Jampilek, Heterocycles in medicinal chemistry, Molecules 24 (2019) 3839, https://doi.org/10.3390/molecules24213839.
[11] S. Kumar, S.L. Khokra, A. Yadav, Triazole analogues as potential pharmacological agents: a brief review, Futur. J. Pharm. Sci. 7 (2021) 106–127, https://doi.org/10.1186/s43094-021-00241-3.
[12] C.H. Zhou, Y. Wang, Recent researches in triazole compounds as medicinal drugs, Curr. Med. Chem. 19 (2012) 239–280, https://doi.org/10.2174/092986712803414213.
[13] R. Kharb, P.C. Sharma, M.S. Yar, Pharmacological significance of triazole scaffold, J. Enzyme Inhib. Med. Chem. 26 (2011) 1–21, https://doi.org/10.3109/14756360903524304.
[14] M. Juricek, P.H.J. Kouwera, A.E. Rowan, Triazole: a unique building block for the construction of functional materials, Chem. Comm. 47 (2011) 8740–8749, https://doi.org/10.1039/C1CC10685F.
[15] R. Kaur, A. Ranjan Dwivedi, B. Kumar, V. Kumar, Recent developments on 1,2,4-triazole nucleus in anticancer compounds: a review, Anti Cancer Agents Med. Chem. 16 (2016) 465–489, https://doi.org/10.2174/1871520615666150819121106.
[16] F. Gao, T. Wang, J. Xiao, G. Huang, Antibacterial activity study of 1,2,4-triazole derivatives, Eur. J. Med. Chem. 173 (2019) 274–281, https://doi.org/10.1016/j.ejmech.2019.04.043.
[17] DrS.A. El-Sebaey, Recent advances in 1,2,4-triazole scaffolds as antiviral agents, ChemistrySelect 8 (2020) 11654–11680, https://doi.org/10.1002/slct.202002830.
[18] R. Sathyanarayana, B. Poojary, Exploring recent developments on 1,2,4-triazole: synthesis and biological application, J. Chin. Chem. Soc. 67 (2020) 459–477, https://doi.org/10.1002/jccs.201900304.
[19] H.-Z. Zhang, G.L.V. Damu, G.-X. Cai, C.-H. Zhou, Current developments in the syntheses of 1,2,4-triazole compounds, Curr. Org. Chem. 18 (2014) 349–406, https://doi.org/10.2174/1385272813179990025.
[20] Y.A. Al-Soud, M.N. Al-Dweri, N.A. Al-Masoudi, Synthesis, antitumor and antiviral properties of some 1,2,4-triazole derivatives, Farmaco 59 (2004) 775–783, https://doi.org/10.1016/j.farmac.2004.05.006.
[21] M.V. Slivka, N.I. Korol, M.M. Fizer, Fused bicyclic 1,2,4-triazoles with one extra sulfur atom: synthesis, properties, and biological activity, J. Heterocycl. Chem. 57 (2020) 3236–3254, https://doi.org/10.1002/jhet.4044.
[22] N. Korol, O.M. Holovko-Kamoshenkova, M. Slivka, O. Pallah, M.Yu Onysko, A. Kryvovyaz, N. Boyko, O.V. Yaremko, R. Mariychuk, Synthesis, biological evaluation and molecular docking studies of novel series of bis-1,2,4-triazoles as thymidine phosphorylase inhibitor, Adv. Appl. Bioinform. Chem. 16 (2023) 39–102, https://doi.org/10.2147/AABC.S415961.

[23] M. Slivka, N. Korol, V. Pantyo, V. Baumer, V. Lendel, Regio- and stereoselective synthesis of [1,3]thiazolo[3,2-b][1,2,4]triazol-7-ium salts via electrophilic heterocyclization of 3-S-propargylthio-4H-1,2,4-triazoles and their antimicrobial activity, Heterocycl. Commun. 23 (2017) 109–113, https://doi.org/10.1515/hc-2016-0233.

[24] M. Slivka, M. Fizer, R. Mariychuk, M. Ostafin, O. Moyzesh, G. Koval, O. Holovko-Kamoshenkova, I. Rusyn, V. Lendel, Synthesis and antimicrobial activity of functional derivatives of thiazolo[2,3-c][1,2,4]triazoles, Lett. Drug Des. Discov. 19 (2022) 791–799. https://www.eurekaselect.com/article/120070.

[25] M. Slivka, N. Korol, Synthesis of mononuclear heterocycles via electrophilic cyclization, Monatsh. Chem. 153 (2022) 1–8, https://doi.org/10.1007/s00706-021-02869-6.

[26] M. Slivka, M. Onysko, The use of electrophilic cyclization for the preparation of condensed heterocycles, Synthesis 53 (2021) 3497–3512, https://doi.org/10.1055/s-0040-1706036.

[27] N. Korol, M. Slivka, M. Fizer, V. Baumer, V. Lendel, Halo-heterocyclization of butenyl(prenyl)thioethers of 4,5-diphenyl-1,2,4-triazol-3-thiole into triazolo[5,1-b] [1,3]thiazinium systems: experimental and theoretical evolution, Monatsh. Chem. 151 (2020) 191–198, https://doi.org/10.1007/s00706-019-02545-w.

[28] M. Slivka, N. Korol, M. Fizer, V. Baumer, V. Lendel, Thiazolo[3,2-b][1,2,4]triazol-7-ium salts: synthesis, properties and structural studies, Heterocycl. Commun. 24 (2018) 197–203, https://doi.org/10.1515/hc-2018-0048.

[29] M. Slivka, N. Korol, I. Rusyn, V. Lendel, Synthesis of [1,3]thiazolo[3,2-b][1,2,4]triazol-7-ium and [1,2,4]triazolo[5,1-b][1,3]thiazin-4-ium salts via regioselective electrophilic cyclization of 3-[(2-alken-1-yl)sulfanyl]-4H-1,2,4-triazoles, Heterocycl, Commun. Now. 21 (2015) 397–401, https://doi.org/10.1515/hc-2015-0158.

[30] D.L. Stevens, The role of vancomycin in the treatment paradigm, Clin. Infect. Dis. 42 (2006) S51–S57, https://doi.org/10.1086/491714.

[31] D.P. Levine, Vancomycin: a history, Clin. Infect. Dis. 42 (2006) S5–S12, https://doi.org/10.1086/491709.

[32] C.M. Baldwin, K.A. Lyseng-Williamson, S.J. Keam, Meropenem. A review of its use in the treatment of serious bacterial infections, Drugs 68 (2008) 803–838, https://doi.org/10.2165/00003495-200868060-00006.

[33] R.H. Deurenberg, E.E. Stobberingh, The evolution of Staphylococcus aureus, Infect. Genet. Evol. 8 (2008) 747–763, https://doi.org/10.1016/j.meegid.2008.07.007.

[34] P. Gastmeier, Serratia marcescens: an outbreak experience, Front. Microbiol. 5 (2014) 81, https://doi.org/10.3389/fmicb.2014.00081.

[35] O.M. Holovko-Kamoshenkova, N.I. Korol, M.V. Slivka, S.A. Tymoshchuk, N.V. Boyko, Application of fluorine-containing derivatives of 1,2,4-triazoles as bactericides, Patent UA 150880, Database "Inventions (useful models) in Ukraine (2022). https://base.uipv.org/searchINV/search.php?action=viewdetails&IdClaim=281369.

[36] N. Korol, S. Burmei, O. Holovko-Kamoshenkova, M. Slivka, Determination of the antagonistic activity of fluorinecontaining 1,2,4-triazoles, Sci. Bull. Uzh. Univ. Ser. Chem. 51 (2024) 59–63, https://doi.org/10.24144/2414-0260.2024.1.59-63.

[37] S.M.A. Kawsar, S. Munia Nasrin, S. Supriyo, O. Yasuhiro, In silico pharmacokinetics, molecular docking and molecular DynamicsSimulation studies of nucleoside analogs for drug discovery- A mini review, Mini-Rev. Med. Chem. 24 (2024) e101123223412, https://doi.org/10.2174/0113895575258033231024073521.

[38] S.M.A. Kawsar, M.A. Hossain, S. Saha, E.M. Abdallah, A.R. Bhat, S. Ahmed, J. Jamalis, Y. Ozeki, Nucleoside-based drug target with general antimicrobial screening and specific computational studies against SARS-CoV-2 main protease, ChemistrySelect 9 (2024) e202304774, https://doi.org/10.1002/slct.202304774.

[39] S.M.A. Kawsar, M.A. Hosen, S. Ahmad, Y. El Bakri, H. Laaroussi, Potential SARS-CoV-2 RdRp inhibitors of cytidine derivatives: molecular docking, molecular dynamic simulations, ADMET, and POM analyses for the identification of pharmacophore sites, PLoS One 17 (2022) e0273256, https://doi.org/10.1371/journal.pone.0273256.

[40] N.C. Desai, H.V. Vaghani, A.M. Jethawa, V.M. Khedkar, In silico molecular docking studies of oxadiazole and pyrimidine bearing heterocyclic compounds as potential antimicrobial agents, Arch. Pharm. 7 (2021) e2100134, https://doi.org/10.1002/ardp.202100134.

[41] A.C.J. de Araújo, P.R. Freitas, I.M. Araújo, Potentiating-antibiotic activity and absorption, distribution, metabolism, excretion and toxicity properties (ADMET) analysis of synthetic thiadiazines against multi-drug resistant (MDR) strains, Fundam. Clin. Pharmacol. 38 (2024) 84–98, https://doi.org/10.1111/fcp.12950.

[42] O. Trott, A.J. Olson, AutoDock Vina: improving the speed and accuracy of docking with a new scoring function, efficient optimization, and multithreading, J. Comput. Chem. 31 (2010) 455–461, https://doi.org/10.1002/jcc.21334.

[43] Dassault Systèmes BIOVIA, Discovery Studio Visualizer, Release 2021, Dassault Systèmes, San Diego, CA, USA, 2021.

[44] Hyperchem, Inc., Gainesville, FL, USA.

[45] J.C. Phillips, R. Braun, W. Wang, J. Gumbart, E. Tajkhorshid, E. Villa, C. Chipot, R.D. Skeel, L. Kalé, K. Schulten, Scalable molecular dynamics with NAMD, J. Comput. Chem. 26 (2005) 1781–1802, https://doi.org/10.1002/jcc.20289.

[46] https://www.charmm-gui.org/.

[47] B. Knapp, N. Lederer, U. Omasits, W. Schreiner, vmdICE: a plug-in for rapid evaluation of molecular dynamics simulations using VMD, J. Comput. Chem. 31 (2010) 2868–2873, https://doi.org/10.1002/jcc.21581.

[48] http://www.meduniwien.ac.at/msi/biosim/bk/a1375/.

[49] O.M. Holovko-Kamoshenkova, M.V. Slivka, R. Hrdina, V.N. Baumer, N.I. Korol, L.V. Sokolenko, V.G. Lendel, An efficient catalyst-free direct approach to 5-Polyfluoroalkyl-1,2,4-triazole-3-thiones, Synthesis 55 (2023) 1221–1226, https://doi.org/10.1055/s-0042-1751401.

[50] G.Y.C. Cheung, J.S. Bae, M. Otto, Pathogenicity and virulence of *Staphylococcus aureus*, Virulence 12 (2021) 547–569, https://doi.org/10.1080/21505594.2021.1878688.

[51] R. Zivkovic Zaric, M. Zaric, M. Sekulic, N. Zornic, J. Nesic, V. Rosic, T. Vulovic, M. Spasic, M. Vuleta, J. Jovanovic, Antimicrobial treatment of *Serratia marcescens* invasive infections: systematic review, Antibiotics 12 (2023) 367, https://doi.org/10.3390/antibiotics12020367.

[52] D.P. Levine, Vancomycin: a history, Clin. Infect. Dis. 42 (2006) S5–S12, https://doi.org/10.1086/491709.

[53] C.M. Baldwin, K.A. Lyseng-Williamson, S.J. Keam, Meropenem, Drugs 68 (2008) 803–838, https://doi.org/10.2165/00003495-200868060-00006.

[54] https://admetmesh.scbdd.com/.

[55] https://preadmet.webservice.bmdrc.org/adme/.

[56] J. Potempa, J. Travis, 96 - aureolysin, in: A.J. Barrett, N.D. Rawlings, J.F. Woessner (Eds.), Handbook of Proteolytic Enzymes, second ed., Academic Press, 2004, pp. 389–393, https://doi.org/10.1016/B978-0-12-079611-3.50104-X. Reference to a website:.

[57] T.E. Benson, C.T. Walsh, J.M. Hogle, The structure of the substrate-free form of MurB, an essential enzyme for the synthesis of bacterial cell walls, Structure 15 (1996) 47–54, https://doi.org/10.1016/s0969-2126(96)00008-1.

[58] H. Bedouelle, Tyrosyl-tRNA synthetases, in: Madame Curie Bioscience Database, Landes Bioscience, 2000-2013 [Internet], Austin (TX), https://www.ncbi.nlm.nih.gov/books/NBK6553/.

[59] L.P. Yu, S. Xiang, G. Lasso, D. Gil, M. Valle, L. Tong, A symmetrical tetramer for S. aureus pyruvate carboxylase in complex with coenzyme A, Structure 10 (2009) 823–832, https://doi.org/10.1016/j.str.2009.04.008.

[60] J.R. Edwards, Meropenem: a microbiological overview, J. Antimicrob. Chemother. 36 (1995) 1–17, https://doi.org/10.1093/jac/36.suppl_A.1.

[61] C.M. Baldwin, K.A. Lyseng-Williamson, S.J. Keam, Meropenem, Drugs 68 (2008) 803–838, https://doi.org/10.2165/00003495-200868060-00006.

[62] M.B. Brurberg, I.F. Nes, V.G.H. Eijsink, Comparative studies of chitinases A and B from Serratia marcescens, Microbiology 142 (1996) 1581–1589, https://doi.org/10.1099/13500872-142-7-1581.

[63] R.M. Romero, M.F. Roberts, J.D. Phillipson, Anthranilate synthase in microorganisms and plants, Phytochemistry 39 (1995) 263–276, https://doi.org/10.1016/0031-9422(95)00010-5.

[64] A.M. Churchill-Angus, T.H.B. Schofield, T. R Marlow, S.E. Sedelnikova, J.S. Wilson, J.B. Rafferty, P.J. Baker, Characterisation of a tripartite α-pore forming toxin from Serratia marcescens, Sci. Rep. 11 (2021) 6447–6462, https://doi.org/10.1038/s41598-021-85726-0.

[65] V. Biou, R.J.D. Adaixo, M. Chami, P.D. Coureux, B. Laurent, V.Y.N. Enguéné, G.C. de Amorim, N. Izadi-Pruneyre, C. Malosse, J. Chamot-Rooke, H. Stahlberg, P. Delepelaire, Structural and molecular determinants for the interaction of ExbB from Serratia marcescens and HasB, a TonB paralog, bioRxiv 04.21 (2021) 440815, https://doi.org/10.1101/2021.04.21.440815.
[66] https://www.ebi.ac.uk/thornton-srv/software/PDBsum1/.
[67] Z. Zhu, Z. Xu, W. Zhu, Interaction nature and computational methods for halogen bonding: a perspective, J. Chem. Inf. Model. 60 (2020) 2683–2696, https://doi.org/10.1021/acs.jcim.0c00032.
[68] Y. Bouzian, K. Karrouchi, Y. Sert, C.-H. Lai, L. Mahi, N.H. Ahabchane, A. Talbaoui, J.T. Mague, E.M. Essassi, Synthesis, spectroscopic characterization, crystal structure, DFT, molecular docking and in vitro antibacterial potential of novel quinoline derivatives, J. Mol. Struct. 1209 (2020) 127940, https://doi.org/10.1016/j.molstruc.2020.127940.
[69] F. Riaz, MdS. Hossain, M. Roney, Y. Ali, S. Qureshi, R. Muhammad, L.C. Ming, Evaluation of potential bacterial protease inhibitor properties of selected hydroxyquinoline derivatives: an in silico docking and molecular dynamics simulation approach, J. Biomol. Struct. Dyn. 41 (2022) 9756–9769, https://doi.org/10.1080/07391102.2022.2146200.
[70] J.Y. Al-Humaidi, S.M. Gomha, N.A.A. El-Ghany, B. Farag, M.E.A. Zaki, T.Z. Abolibda, N.A. Mohamed, Green synthesis and molecular docking study of some new thiazoles using terephthalohydrazide chitosan hydrogel as ecofriendly biopolymeric catalyst, Catalysts 13 (2023) 1311, https://doi.org/10.3390/catal13091311.
[71] K.B. Patel, R.V. Patel, I. Ahmad, D. Rajani, H. Patel, S. Mukherjee, P. Kumari, Design, synthesis, molecular docking, molecular dynamic simulation, and MMGBSA analysis of 7-O-substituted 5-hydroxy flavone derivatives, J. Biomol. Struct. Dyn. 42 (2023) 6378–6392, https://doi.org/10.1080/07391102.2023.2243520.
[72] O.M.H. Salo-Ahen, I. Alanko, R. Bhadane, A.M.J.J. Bonvin, R.V. Honorato, S. Hossain, A.H. Juffer, A. Kabedev, M. Lahtela-Kakkonen, A.S. Larsen, Molecular dynamics simulations in drug discovery and pharmaceutical development, Processes 9 (2021) 71, https://doi.org/10.3390/pr9010071.
[73] A. Kuzmanic, G.R. Bowman, J. Juarez-Jimenez, J. Michel, F.L. Gervasio, Investigating cryptic binding sites by molecular dynamics simulations, Acc. Chem. Res. 53 (2020) 654–661, https://doi.org/10.1021/acs.accounts.9b00613.
[74] R. Shukla, T. Tripathi, Molecular dynamics simulation of protein and protein–ligand complexes, in: D.B. Singh (Ed.), Computer-Aided Drug Design, Springer, Singapore, 2020, https://doi.org/10.1007/978-981-15-6815-2_7.
[75] C.J. Morris, D.D. Corte, Using molecular docking and molecular dynamics to investigate protein-ligand interactions, Mod. Phys. Lett. B 35 (2021) 2130002, https://doi.org/10.1142/S0217984921300027.